Fachtagung "Experimentelle Strömungsmechanik"
4. – 6. September 2018, Rostock

Bestimmung von Strömungsmustern in einem Zylinderspalt mit radialem elektrischen Kraftfeld unter Schwerelosigkeit

Identification of flow pattern in an annulus with radial electric force field under microgravity conditions

Marcel Jongmanns, Martin Meier, Antoine Meyer, Christoph Egbers
Department of Aerodynamics and Fluid Mechanics
Brandenburg University of Technology (BTU) Cottbus - Senftenberg
LG 3A, Siemens-Halske-Ring 14
D-03046 Cottbus, Germany
Phone: +49(0)355 69 4868
Fax: +49(0)355 69 4891

Schlagworte: Zylinderspalt, Elektrohydrodynamik, Mikrogravitation, Strömungsvisualisierung
Key words: Cylindrical Gap, Electrohydrodynamic, Microgravity, Flow visualization

Abstract

The effect of the dielectrophoretic (DEP) force on a dielectric fluid inside a differentially heated annulus with applied electric a.c. field is examined. The natural buoyancy convection, which acts in laboratory experiments with Earth's gravity, is superimposed by the radially acting electric gravity. In parabolic flight experiments, we found two dominant flow pattern developing during the about 22s of microgravity: an axisymmetric pattern with toroidal vortices and a non-axisymmetric pattern with columnar or helical vortices. This knowledge can be transferred to applications in space to create thermal convections and on earth to control the efficiency of heat exchangers.

Introduction

We are investigating the effect of an a.c. electric field on the flow in a differentially heated annulus. With our experimental setup, it is possible to induce convective flows by utilizing the dielectrophoretic (DEP) force (Pohl 1978, Dahley 2014). The temperature gradient and natural gravity create a thermal buoyancy flow inside the annulus. The DEP force can also be seen as a gravitational force, which can be used to control the convective heat transfer between inner and outer cylinder. A theoretical analysis of this problem is given by Yoshikawa et al. 2013. To study the effect of the pure DEP force, it is required to conduct the experiments in a microgravity (µg) environment. The results of our investigations can be transferred to applications in space to create convective flows in dielectric liquids and on earth to control the efficiency of heat exchangers.

The experiment layout is shown in Fig. 1. The inner cylinder is heated and connected to the phase of a high-voltage amplifier with a peak voltage of up to $V_{peak} = \pm 10kV$ at f=200Hz. The outer cylinder is cooled, and connected to electric ground. The inner cylinder radius R_1 is 5mm, the outer radius R_2 is 10mm. The height H is either H=30mm or H=100mm. The gap is filled with the silicone oil AK5.

Karlsruhe, Germany, ISBN 978-3-9816764-5-7

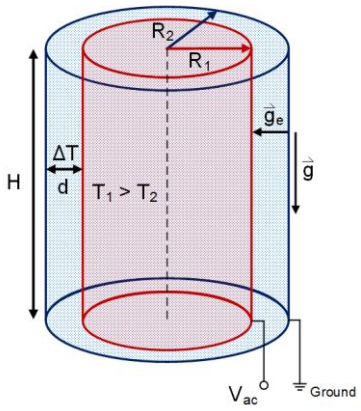

Figure 1: Layout of the experiment cell.

When a temperature gradient ΔT, but no voltage, is applied, then a unicellular convective flow is seen inside the gap, see Figure 2, left. This flow is driven by the density differences caused by the heating and the natural gravity **g**. The temperature gradient also causes a gradient of the permittivity **ε** of the fluid. When an a.c. voltage is applied, an artificial gravity $\mathbf{g_e}$ is created (Fig. 2, middle). The colder fluid, which has an increased **ε**, is moved towards the region, where the electric field has a higher field strength. Because of the cylindrical geometry, this is at the inner cylinder. In µg, when only $\mathbf{g_e}$ influences the flow, a completely different pattern with toroidal vortices is observed (Fig. 2, right). Since $\mathbf{g_e}$ is always superimposed by **g** inside the laboratory, we performed experiments in parabolic flights campaigns (PFC) to investigate the flow in µg when only $\mathbf{g_e}$ acts on it.

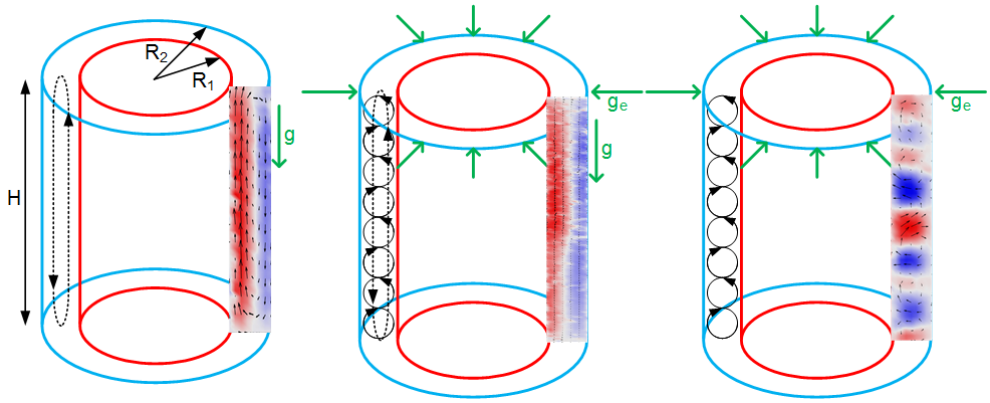

Figure 2: The effect of the earth's gravity and electric gravity in a differentially heated annulus. The experimental images shown at the right of the annuli are acquired by PIV.

The parabolic maneuver involves 5 different phases. After the steady-flight (1g) follows the 1.8g pull-up phase with ~20s leading to the free fall or µg phase which lasts ~ 22s, followed by a 1.8g pull-out phase of ~20s and finally steady-flight phase again. This is done about 30 times per flight day and there are 3 to 4 flight days per PFC. Between the parabolas is a break of 1 to 15 minutes, which allows the experimenters to change the settings of their experiments. Because of the limited time in the µg phase, usually about 20 to 22s, and the preceding 1.8g phase, the flow will maybe not enter a stable state during the µg experiments. However, it changes fast enough to get a reliable and repeatable result in which way the flow state changes. Depending on the experimental settings, different instabilities can be found, e.g. an axisymmetric pattern with toroidal vortices along the azimuthal direction or a non-axisymmetric

Karlsruhe, Germany, ISBN 978-3-9816764-5-7

pattern with columnar vortices in the axial direction. In the latter case, it is also possible to have slanted columns (Yoshikawa et al. 2013). The flow is visualized by Shadowgraph, Synthetic Schlieren and PIV methods. Due to the electric field, the chosen methods are non-invasive, principally. Ideal tracer particles for the PIV measurements should not only have the same density as the fluid, but also the same permittivity and may not be made of electric conducting materials or interfere with the electric field in any other way. By using the DEP force, it is possible to control the flow inside the gap of the annulus and to invoke convective heat transfer under µg conditions (Dahley et al. 2016, and Meyer et al. 2017).

Experimental setup

The experimental setup is divided into two racks with several, modular parts. This allows an easy and quick exchange of components. The PC and data acquisition hardware are installed at the Control Rack, and the Experiment Rack includes the Experiment Box and several electric auxiliary devices needed to supply the experiment. There is one Experiment Box type “P” designed for PIV measurements and one type “T” designed for Shadowgraph/ Synthetic Schlieren and temperature field measurements. As an example of such a setup, the inside of the PIV measurement Experiment Box is shown in Fig. 3. A more detailed description can be found in Meier et al. 2016.

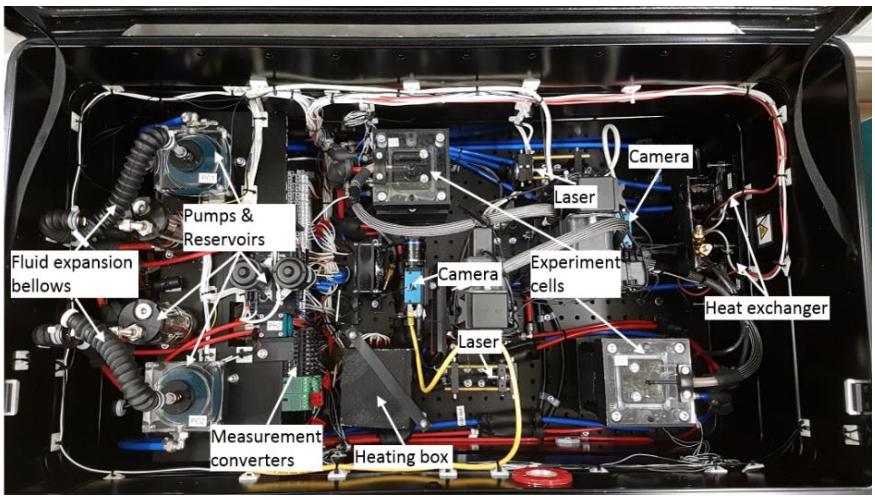

Figure 3: View into the Experiment Box for PIV measurements. Two experiment cells, one with H=30mm and one with H=100mm, are used at the same time.

Shadowgraph method

The evaluation of the Shadowgraph images is done as described by Schöpf et al.1996. The light intensity of the experimentally obtained image (see Fig. 5) is correlated to the light intensity of a reference image by $I = \frac{I_{measured}}{I_{reference}}$. I is the light intensity given by the gray level of the

Karlsruhe, Germany, ISBN 978-3-9816764-5-7

camera images. The light beams are bent towards the cold fluid. The setup for the Shadowgraph and Synthetic Schlieren methods is shown in Fig. 4. It consists of a LED panel with light control films located below the cell. For the Synthetic Schlieren method, below the cell is also a mask with a random dot pattern. The image is captured from above by a camera via a 45° surface mirror.

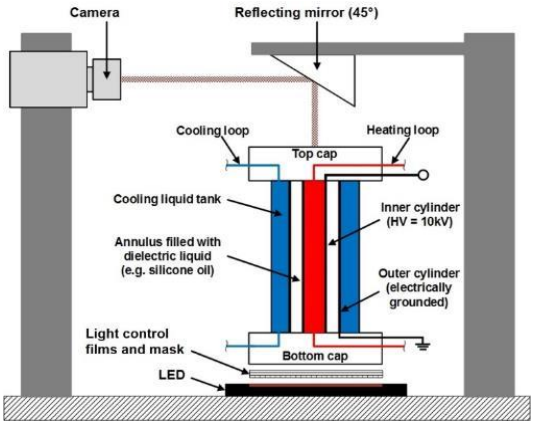

Figure 4: Sketch of the setup for the Shadowgraph and the Synthetic Schlieren method.

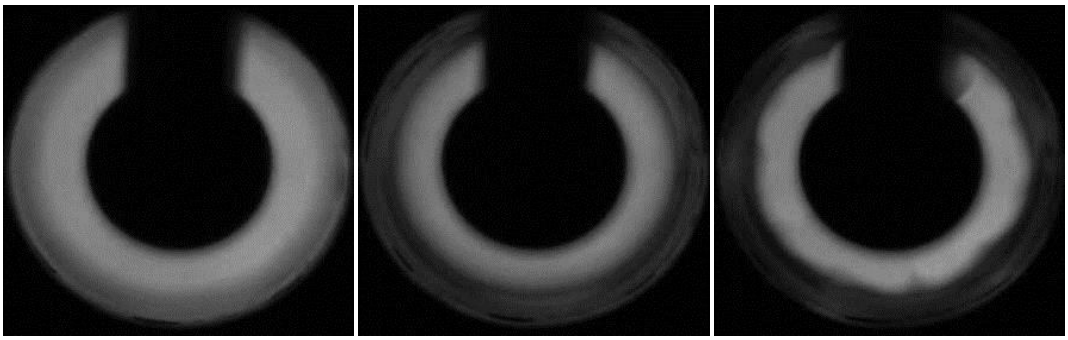

Figure 5: Acquired images (one experimental run). Left: No temperature gradient nor voltage applied. Middle: Temperature gradient, but no voltage is applied. Right: A temperature gradient and voltage is applied.

As reference for the evaluation, an image of the annulus with applied temperature difference showing the base state, but without applied voltage is used. This puts an emphasis on the changes caused by the electric field und reduces the impact caused by the heating. The evaluation of the right image in Fig. 5 with the middle image of Fig. 5 as reference gives the result shown in Fig. 6.

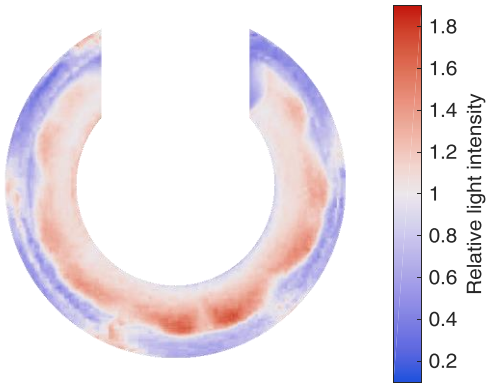

Figure 6: Evaluated Shadowgraph image.

Karlsruhe, Germany, ISBN 978-3-9816764-5-7

The vaguely visible dents in Fig. 5 are now enhanced and easier to see. These structures are caused by jets of hot fluid going to the outer cylinder. It is possible to count the low intensity parts at the outer cylinder, which are divided by high intensity jets. In Fig. 6 this would give an azimuthal mode number of n=6. It also suggests that there is a non-axisymmetric, columnar-like flow pattern inside the gap.

Synthetic Schlieren method

The Synthetic Schlieren method is based on the fact, that the refraction inside a fluid changes the appearance of a given pattern (Dalziel et al. 2000).
In our experiments, we use a mask with a random dot pattern. The evaluation is performed by a cross-correlation similar to PIV. In contrast to PIV, the results do not describe a velocity field, but a displacement field.

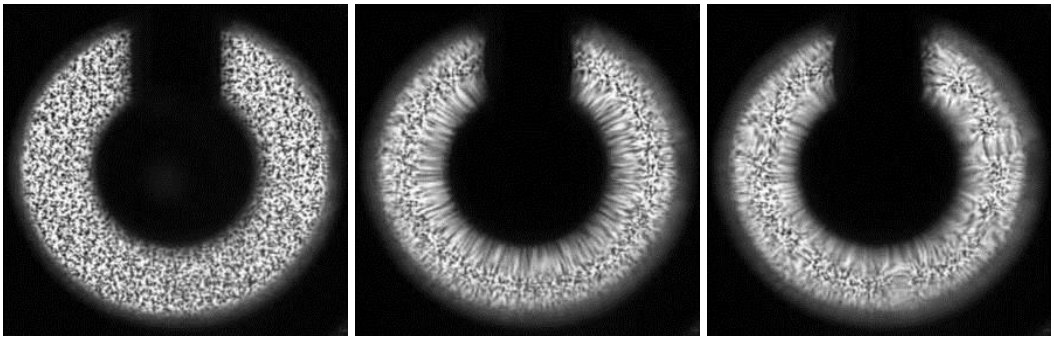

Figure 7: Acquired images (one experimental run). Left: No temperature gradient, no voltage applied. Middle: Temperature gradient, no voltage. Right: Temperature gradient and voltage applied.

Fig. 7 shows experimental images with different parameters. The left image without temperature gradient nor applied voltage shows the undistorted mask. After applying a temperature gradient (middle), the mask near the inner cylinder shows a substantial blur. The outer region is only slightly distorted. When also an electric field is applied (right), the blur near the inner cylinder decreases, but some blurred spots appear in the gap (e.g. bottom center of the gap). While some blurred spots can be seen by eye, others become recognizable only after the cross-correlation process. The cross-correlation is performed between the experimental image with temperature gradient and voltage (Fig. 7 right), and the picture of the heated state without applied voltage (Fig. 7 middle). The image and reference are chosen in this way to neglect the impact of the temperature gradient and put emphasis on the changes caused by the electric field.

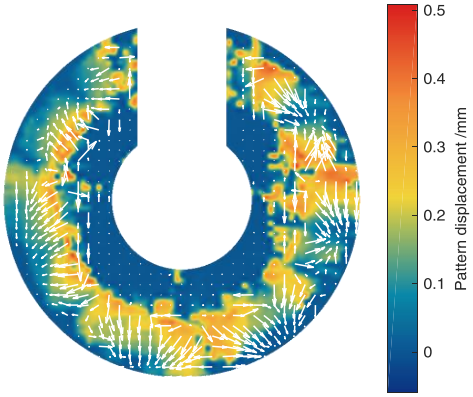

Figure 8: The result of a cross-correlation between the right and middle image of Fig. 7.

Karlsruhe, Germany, ISBN 978-3-9816764-5-7

The result of this correlation is shown in Fig. 8. The colors give the magnitude of the displacement. The vector field has several spots, at which the vectors converge near the outer cylinder. These are the cold regions, comparable to the blue spots in the Shadowgraph images. Between these regions are diverging vectors, which are the hot fluid jets. Counting these structures gives the azimuthal mode number, which is n=7 in this case.

Laser-Light Sheet/ Particle Imaging Velocimetry

The Laser-Light Sheet/ PIV setup includes a continuous line laser and a camera mounted perpendicular to the laser sheet (Fig. 9). The laser-light sheet is generated by a continuous line laser source. It is aligned to the center of the gap.

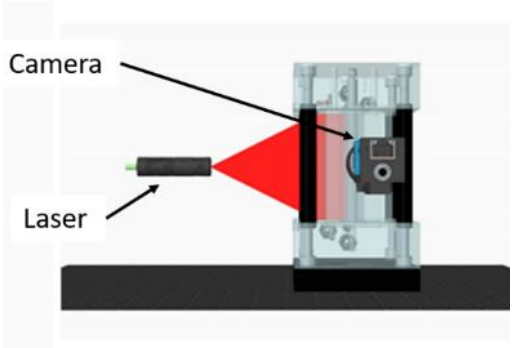

Figure 9: Sketch of the setup for the Laser-Light Sheet/ PIV technique.

The images are acquired at 10 Hz by a camera, which is mounted perpendicular to the laser sheet. Hollow Glass Spheres are used as tracer particles. They fit very well based on their density and permittivity to the silicone oil and show no remarkable interference with the high electric field. The images are evaluated in Matlab using the PIVlab toolbox (Thielicke and Stamhuis 2014). A multi iteration function is used with an interrogation window size of 32x32 and 16x16 pixels and a 75% overlap. The used time step between the images depends on the experiment settings, since the velocity ranges from nearly 0 mm/s to about 4 mm/s with high temperature gradients and voltages.

Results

Due to the missing gravitational force, there is no thermal buoyancy in a µg environment. The velocity field in the PIV images becomes zero, and the Shadowgraph and Synthetic Schlieren images produce a nearly homogeneous result. A purely conductive state will appear where the heat is transferred from the inner to the outer cylinder only by conduction. By applying an electric a.c. field to the dielectric fluid, the cold fluid from the outer cylinder is moved towards the inner cylinder, because the cold fluid has a higher permittivity and the non-uniform electric field is at strongest at the inner cylinder. This creates a convective thermoelectric flow in µg.

Karlsruhe, Germany, ISBN 978-3-9816764-5-7

For the 100mm cell, the preferred instabilities are non-axisymmetric (Fig. 10). The results from the PIV images show toroidal vortices near the top and bottom caps of the cells. This is caused by boundary effects. The artificial gravity causes an inward flow of the cold oil from the outer cylinder, which also causes a mass flow of the hot oil towards the outer cylinder. This creates vortices, which can be seen in the Shadowgraph image. This image shows a pattern with alternating brighter and darker parts at the outer cylinder. This indicates a columnar-like flow pattern. The brighter parts are caused by the hot jets of the fluid moving to the outer cylinder. The darker, oval spots near the outer cylinder are the region where the oil cools down. The inward flow of the cold fluid cannot be seen at this temperature gradient in the Shadowgraph image. The PIV image also shows a change of the sign of the radial direction of the fluid. This indicates a helical pattern. Combining both results, we can conclude that this is a flow pattern with helical columns.

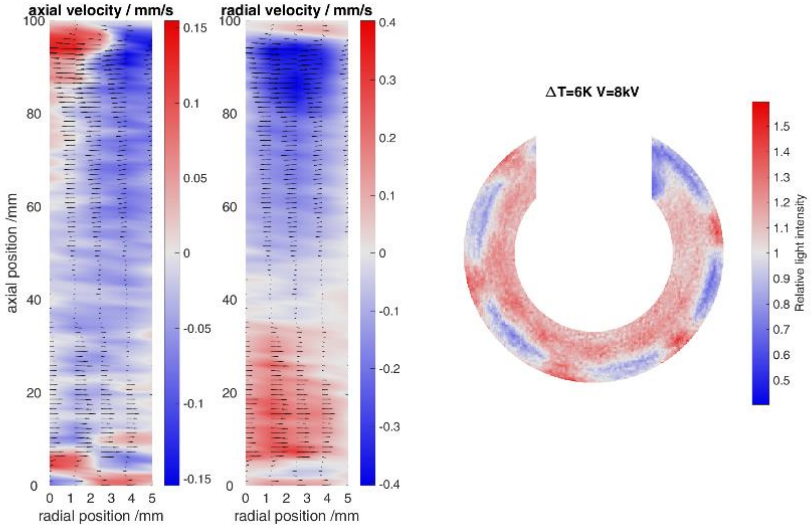

Figure 10: Experimental results of 100mm cell in µg; $\Delta T = 6K$, $V_{peak} = 8kV$.

The flow in the 30mm cell shows a different behavior. Similar to the 100mm cell, there is no flow in µg, when the voltage is too low. After a first critical voltage, there is an axisymmetric instability, which cannot be seen in the 100mm cell. The axisymmetric pattern (Fig. 11) is defined by toroidal vortices over the whole height of the gap. Since these structures can only be seen on the boundaries in the 100mm cell, it can be assumed that the strong boundary effects in the 30mm cell promote this structure. The corresponding Synthetic Schlieren image shows no specific structure. The refractions of the light beams result in a zigzag pattern for the toroidal pattern. Integrating over this zigzag pattern results in a homogeneous pattern of the Synthetic Schlieren image.

The evaluation process is supported by a linear stability analysis (LSA) (Yoshikawa et al. 2013). This predicts critical parameters at which the flow pattern changes (Fig. 12, blue line). In microgravity, it is predicted to see a helical instability within the critical parameters. The parameters are given by the dimensionless electric potential $V_E = V_{RMS}\left[\sqrt{\frac{\rho\nu\kappa}{\varepsilon_0\varepsilon_r}}\right]^{-1}$ with $V_{RMS} = \frac{V_{peak}}{\sqrt{2}}$, density ρ, kinematic viscosity ν, thermal diffusivity κ, relative permittivity ε_r and the permittivity in a vacuum ε_0 , and the non-dimensional temperature gradient $\gamma_e = e\Delta T$ with temperature gradient ΔT and thermal coefficient of permittivity $e = 1.065 \cdot 10^{-3}K^{-1}$ for the used fluid.

Karlsruhe, Germany, ISBN 978-3-9816764-5-7

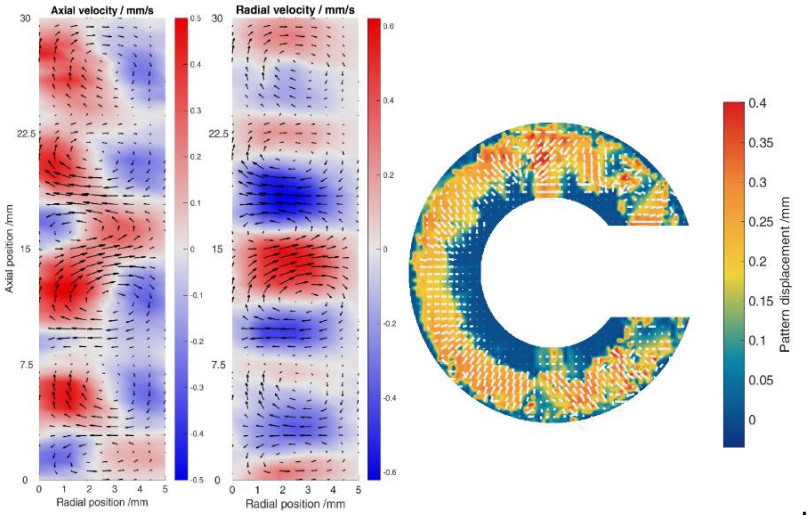

Figure 11: Experimental results of 30mm cell in µg; $\Delta T = 11K$, $V_{peak} = 7kV$.

The LSA assumes a cell of infinite height. Since the 30mm cell is dominated by boundary effects, a comparison is not suitable. For the 100mm cell, the experimental results fit reasonably well to the calculations (Fig. 12). We found the transition to a helical pattern for some parameters. At the other parameters, we found a columnar pattern instead of the helical pattern. This is usually found when the experimental parameters are near the critical parameters. The results of the LSA and the experiments fit reasonably well within the technical limits of the PFC and assumptions like Boussinesq's approximations of the LSA. For lower γ_e it fits quite well, but due to the limited time in the microgravity phase, the flow might not have enough time to reach a stable state. For $\gamma_e > 0.005$ the differences between the stability range calculated by the LSA and our experiments become bigger.

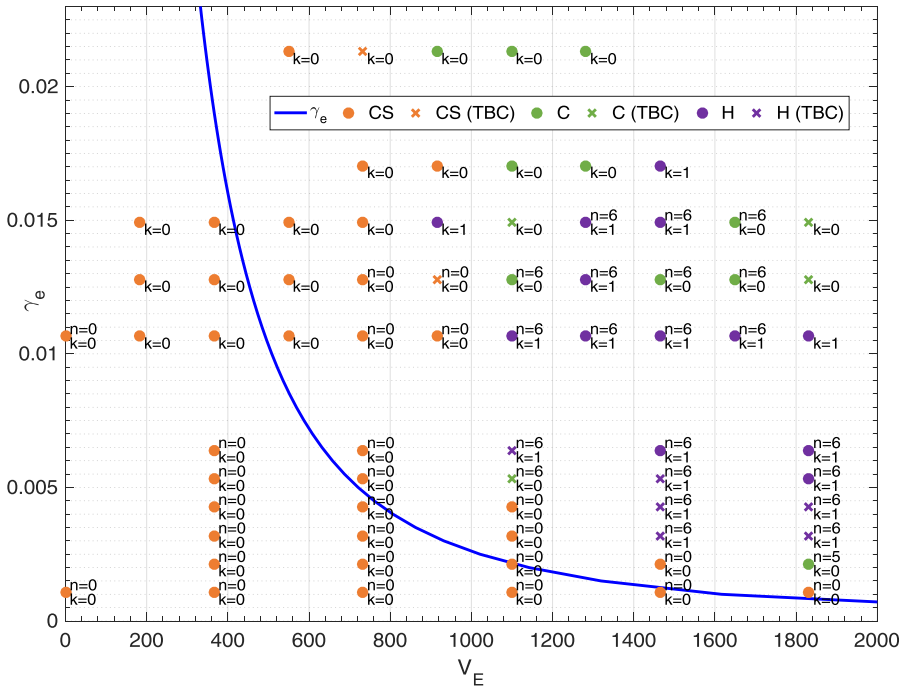

Figure 12: Comparison of the critical parameters predicted by LSA (blue line) to the obtained experimental results. CS-conductive state, C-columnar, H-helical, TBC-to be confirmed.

Summary

We have developed a modular experimental setup for TEHD-investigations in a parabolic flight environment and in the laboratory. We implemented different non-invasive measurement techniques. These techniques allow us to qualify a complex 3D flow by combining two 2D measurement techniques. Two experiment cells with different heights have been used. The cell with 30mm height shows no instabilities in laboratory experiments. However, in µg two different instabilities can be found. The first is an axisymmetric pattern with toroidal vortices inside the annulus. At higher voltages ($V_{peak} \approx 7 \dots 8kV$ for $\Delta T > 9K$), this changes to a non-axisymmetric pattern with columnar vortices as dominant flow. In the 100mm cell, the axisymmetric pattern cannot be found. There is only a non-axisymmetric instability, in 1g as well as µg. The transition occurs at lower voltages in µg, since the buoyancy convection is missing. It is planned to combine PIV and Shadowgraph/Synthetic Schlieren into one setup, so they can be used at the same time. Long time experiments in µg with a TEXUS sounding rocket are planned as well.

Acknowledgement

The project “Untersuchungen zur thermischen Konvektion im konzentrischen Spalt mit elektrischem Zentralkraftfeld unter verminderter Schwerkraft (KIKS)” is funded by the BMWi via the German Aerospace Center DLR (grant no. 50WM1644).

Literature

Dahley, N., 2014: Dielectrophoretic flow control of thermal convection on cylindrical geometries, PhD Thesis BTU Cottbus-Senftenberg, Cuvillier Verlag Göttingen ISBN-13 978-3-73694-863-1

Dalziel, S. B., Hughes, G. O., Sutherland, B. R., 2000: Whole-field density measurements by ‘Synthetic Schlieren’, Exp. Fluids 28, 322–335

Meier, M., Jongmanns, M., Egbers, C., 2016: Untersuchungen zur thermoelektrohydrodynamischen Konvektion im Zylinderspalt, Experimentelle Strömungsmechanik, ISBN: 978-3-9816764-2-6

Meyer, A., Jongmanns, M., Meier, M., Egbers, C., Mutabazi, I., 2017: Thermal convection in a cylindrical annulus under a combined effect of the radial and vertical gravity, C. R. Mécanique 345, 11–20

Pohl, H. A., 1978: Dielectrophoresis, Cambridge University Press, Cambridge, ISBN: 0 521 21657

Schöpf, W., Patterson, J. C., Brooker, A. M. H., 1996: Evaluation of the Shadowgraph method for convective flow in a side-heated cavity, Exp. Fluids 21, 331

Thielicke, W., Stamhuis, E.J., 2014: PIVlab – Towards User-friendly, Affordable, and Accurate Digital Particle Image Velocimetry in MATLAB. Journal of Open Research Software 2 DOI: http://dx.doi.org/10.5334/jors.bl

Yoshikawa, H.N., Crumeyrolle, O., Mutabazi, I, 2013: Dielectrophoretic force-driven thermal convection in annular geometry, Phys. Fluids 25, 024106

Karlsruhe, Germany, ISBN 978-3-9816764-5-7